RESEARCH ARTICLE SUMMARY

SYNTHETIC BIOLOGY

Synthetic multistability in mammalian cells

Ronghui Zhu, Jesus M. del Rio-Salgado, Jordi Garcia-Ojalvo, Michael B. Elowitz*

INTRODUCTION: Multistability allows genetically identical cells to exist in thousands of molecularly distinct and mitotically stable states. Building synthetic multistable circuits could provide insight into the minimal circuitry sufficient for multistability and establish a foundation for exploiting multicellularity in engineered cell therapies. However, efforts in mammalian cells have been limited to two-state systems or have used architectures that cannot be easily expanded. Beyond generating long-term multistability, an ideal synthetic architecture would also recapitulate key properties of natural cell fate control systems, including the ability to switch cells among states with transient external inputs, control the stability of particular states, and generate irreversible state transitions. Despite much work on identifying key genes and regulatory interactions in many natural cell fate control systems, it has remained unclear what circuit architectures could provide these capabilities.

RATIONALE: Natural cell fate control systems exhibit two prevalent features: positive autoregulation and combinatorial protein-protein interactions. We designed a minimal circuit architecture based on similar principles, called MultiFate, in which a set of transcription factors competitively homo- and heterodimerize, with only the homodimers activating the expression of their own gene. Mathematical modeling showed that MultiFate can produce diverse types of multistability, support controlled state switching, and enable irreversible state transitions. Critically, the use of heterodimerization to implement cross-inhibition allows the expansion of MultiFate to larger numbers of states simply by adding new transcription factors, without the need to reengineer existing components. These properties suggest that MultiFate could provide an ideal synthetic architecture for multistability.

RESULTS: To create MultiFate circuits, we first engineered a set of zinc finger transcription factors that enable homodimer-dependent self-activation and heterodimer-dependent inhibition. We then constructed a minimal circuit termed MultiFate-2 (comprising two of these factors), stably integrated it into CHO-K1 cells, and obtained several monoclonal MultiFate-2 cell lines. Flow cytometry and time-lapse imaging showed that MultiFate-2 cells could exist in three distinct expression states, expressing predominantly one factor, the other, or both. Each of these states was stable for extended time scales of weeks or more. Using external inducers, we were able to switch cells among states. Finally, consistent with model predictions, reducing protein stability resulted in a tristable-to-bistable bifurcation, selectively destabilizing the state expressing both factors while preserving states expressing single factors. Cells exiting the destabilized state did not return even when protein stability was restored, recapitulating irreversible state transitions observed in many natural fate control systems.

To test the expandability of the MultiFate design, we integrated a third transcription factor into a MultiFate-2 cell line. As predicted by the model, the resulting MultiFate-3 cells could stably exist in seven distinct states for more than 18 days. Progressively reducing protein stability repeatedly bifurcated the system from septastability through hexastability to tristability, further recapitulating the progressive loss of cell fate potential in natural cell differentiation systems. Modeling indicates that the MultiFate system should be expandable beyond three transcription factors to generate hundreds of robust stable states.

CONCLUSION: Recently, single-cell transcriptomic approaches have revealed a stunning diversity of natural cellular states, making the question of how such multistability is generated and controlled more urgent than ever. MultiFate demonstrates how a relatively simple, naturally inspired architecture can produce several hallmarks of natural multistability: They generate long-term multistability through combinations of transcription factors; they allow controlled state switching using external inducers; and they permit modulation of state stability, which allows hierarchical and irreversible cellular transitions. Because MultiFate can be readily expanded to generate more states by adding new transcription factors, it provides a scalable foundation for exploring circuit-level principles of multistability and enables multicellular applications in synthetic biology. ■

The list of author affiliations is available in the full article online.
*Corresponding author. Email: melowitz@caltech.edu
Cite this article as R. Zhu *et al.*, *Science* **375**, eabg9765 (2022). DOI: 10.1126/science.abg9765

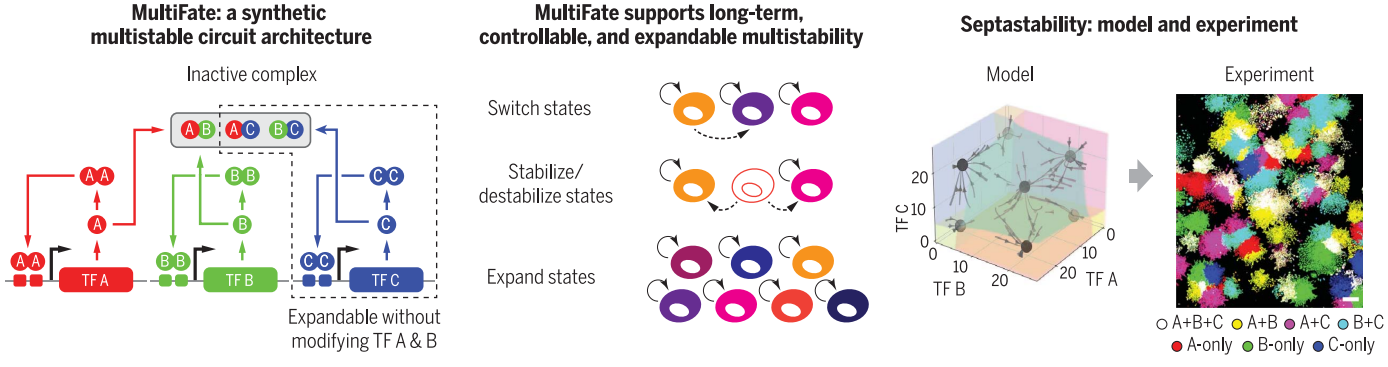

MultiFate supports long-term, controllable, and expandable multistability. Left: In MultiFate, transcription factors (TFs) homodimerize to self-activate and mutually inhibit one another through heterodimerization. Cross-inhibition through heterodimerization allows circuit expansion by adding additional transcription factors without modifying existing components. Center: This circuit design supports state switching, modulation of state stability, and expansion of states. Right: A MultiFate-3 circuit with three transcription factors generates seven stable states (attractors in phase diagram). Experiments show that these seven states, indicated by distinct transcription factor combinations (colors), are stably maintained as cells grow into colonies.

RESEARCH ARTICLE

SYNTHETIC BIOLOGY

Synthetic multistability in mammalian cells

Ronghui Zhu[1], Jesus M. del Rio-Salgado[1], Jordi Garcia-Ojalvo[2], Michael B. Elowitz[1,3]*

In multicellular organisms, gene regulatory circuits generate thousands of molecularly distinct, mitotically heritable states through the property of multistability. Designing synthetic multistable circuits would provide insight into natural cell fate control circuit architectures and would allow engineering of multicellular programs that require interactions among distinct cell types. We created MultiFate, a naturally inspired, synthetic circuit that supports long-term, controllable, and expandable multistability in mammalian cells. MultiFate uses engineered zinc finger transcription factors that transcriptionally self-activate as homodimers and mutually inhibit one another through heterodimerization. Using a model-based design, we engineered MultiFate circuits that generate as many as seven states, each stable for at least 18 days. MultiFate permits controlled state switching and modulation of state stability through external inputs and can be expanded with additional transcription factors. These results provide a foundation for engineering multicellular behaviors in mammalian cells.

Multistability allows genetically identical cells to exist in thousands of molecularly distinct and mitotically stable cell types or states (*1*, *2*). Understanding natural multistable circuits and engineering synthetic ones have been long-standing challenges in developmental and synthetic biology (*3*–*14*). Building synthetic multistable circuits could provide insight into the minimal circuitry sufficient for multistability and would establish a foundation for exploiting multicellularity in engineered cell therapies. However, efforts in mammalian cells have been limited to two-state systems or have used architectures that cannot be easily expanded to larger numbers of states (*5*–*7*). An ideal synthetic multistable system would allow cells to remain in any of a set of distinct expression states over many cell cycles, despite biological noise. In addition, it would provide three key capabilities exhibited by its natural counterparts (Fig. 1A): (i) It would permit transient external inputs to switch cells between states, similar to the way in which signaling pathways direct fate decisions (*15*, *16*). (ii) It would support control over the stability of different states and would enable irreversible transitions, similar to those that occur during natural differentiation (*13*, *14*). (iii) It would be expandable by introducing additional components without reengineering an existing functional circuit, analogous to the expansion of cell types during evolution (*17*).

Natural mammalian multistable circuits provide inspiration for such a synthetic architecture. In many natural fate control systems, transcription factors positively autoregulate their own expression and competitively interact with one another to form a variety of homodimers, heterodimers, and higher-order multimeric forms (Fig. 1B) (*18*–*24*). For example, during myogenesis, muscle regulatory factors such as MyoD heterodimerize with E proteins to activate their own expression and the broader myogenesis program, while Id family proteins disrupt this process through competitive dimerization (*23*, *24*). Similarly, during embryogenesis, Sox2 and Sox17 competitively interact with Oct4 to control fate decisions between pluripotency and endodermal differentiation (*21*, *22*). Related combinations of positive autoregulation and cross-inhibition could extend multistability behaviors beyond bistability and generate bifurcation dynamics that explain the partial irreversibility of cell differentiation (*9*, *12*). Nonetheless, it remains unclear whether these natural architectures could be adapted to enable synthetic multistability. Here, we show how a synthetic multistable system based on principles derived from natural cell fate control systems can generate robust, controllable, expandable multistability in mammalian cells.

MultiFate generates diverse types of multistability through a set of promiscuously dimerizing, autoregulatory transcription factors

Inspired by natural fate control circuits, we designed a new synthetic multistable system called MultiFate. In MultiFate, transcription factors share a common dimerization domain, allowing them to competitively form both homodimers and heterodimers. The promoter of each transcription factor gene contains binding sites that can be strongly bound only by their own homodimers, allowing homodimer-dependent self-activation. By contrast, heterodimers do not efficiently bind to any promoter in this design. Heterodimerization thus acts to mutually inhibit the activity of both constituent transcription factors.

Mathematical modeling shows how the MultiFate architecture provides each of the desired capabilities described above (Fig. 1A) in physiologically reasonable parameter regimes (Box 1 and table S1) (*25*). A MultiFate circuit with just two transcription factors, designated MultiFate-2, can produce diverse types of multistability containing two, three, or four stable fixed points, depending on protein stability and other parameter values (Fig. 1C and fig. S1A). In particular, a regime designated type II tristability is analogous to multilineage priming in uncommitted progenitor cells, with the double positive state playing the role of a multipotent progenitor (*26*–*28*). Transient expression of one transcription factor can switch cells between states (fig. S3 and movie S1). Reducing the protein stability of transcription factors can cause bifurcations that selectively destabilize certain states (Fig. 1C and fig. S1A). Finally, the model is expandable: Addition of a new transcription factor to the MultiFate-2 model generates a MultiFate-3 circuit that supports additional stable states with the same parameter values (Fig. 1D and fig. S2A). Together, these modeling results suggest that the MultiFate architecture can support a rich array of multistable behaviors.

Engineered zinc finger transcription factors enable homodimer-dependent self-activation and heterodimer-dependent inhibition

Synthetic zinc finger (ZF) transcription factors provide an ideal platform to implement the MultiFate circuit. They can recognize and activate a promoter containing target DNA binding sites with high specificity (*29*, *30*). Further, engineered ZF DNA binding domains containing three fingers bind weakly as monomers to 9–base pair (bp) target sites but can bind much more strongly as homodimers to 18-bp tandem binding-site pairs (*31*, *32*). This property allows homodimer-dependent transcriptional activity and potentially allows inhibition through heterodimerization.

To engineer ZF transcription factors, we fused the ErbB2 ZF DNA binding domain to a GCN4 homodimerization domain and a VP48 transcriptional activation domain to create the synthetic transcription factor, termed ZF-GCN4-AD (Fig. 2A) (*31*). A transcription factor (ZF-AD) lacking GCN4 was used as a monomeric control. To assay their transcriptional activity, we constructed a reporter containing 18-bp homodimer binding sites driving the expression of Citrine (*31*). We then cotransfected each transcription factor, together with the reporter and an mTagBFP2 (*33*) cotransfection

[1]Division of Biology and Biological Engineering, California Institute of Technology, Pasadena, CA 91125, USA. [2]Department of Experimental and Health Sciences, Universitat Pompeu Fabra, 08003 Barcelona, Spain. [3]Howard Hughes Medical Institute, California Institute of Technology, Pasadena, CA 91125, USA.
*Corresponding author. Email: melowitz@caltech.edu

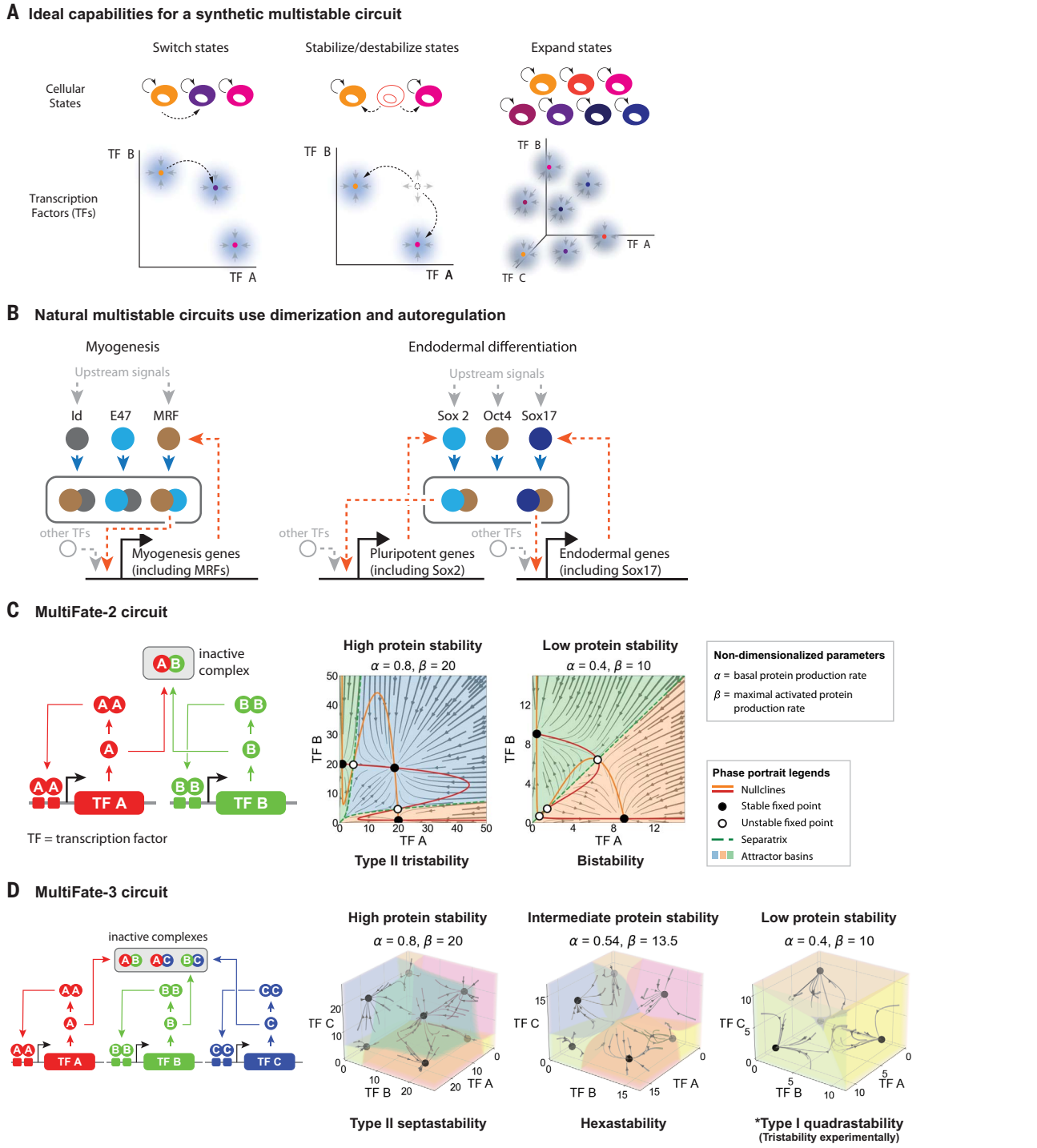

Fig. 1. The naturally inspired MultiFate architecture generates diverse types of multistability in the model. (**A**) A hypothetical synthetic multistable circuit is represented by colored cell cartoons (top) and attractors in a transcription factor phase space (bottom; axes represent transcription factor concentrations of TF A, TF B, and TF C). An ideal synthetic multistable circuit should generate multiple stable states, support control of state switching (left) and state stability (center), and allow easy expansion of states by addition of more transcription factors (right). (**B**) Competitive protein-protein interactions and autoregulatory feedback are prevalent in natural multistable circuits that control myogenesis (left) and endodermal differentiation (right), as shown by these simplified and abridged diagrams. Blue arrows indicate competitive protein-protein interactions, which can involve higher-order multimerization. Orange dashed arrows indicate direct or indirect positive transcriptional feedback. (**C** and **D**) Models of the MultiFate-2 circuit and MultiFate-3 circuit (Box 1) (*25*) generate diverse types of multistability in different parameter regimes (indicated above plots). In the model of the MultiFate-3 circuit, low protein stability generates four stable states (type I quadrastability), but the state in which all transcription factors are minimally expressed is unstable in the presence of biological noise (fig. S22), consistent with experimental results in Fig. 5B, low-TMP columns. See figs. S1 and S2 for complete lists of multistability regimes. All models used here are symmetric and nondimensionalized, with rescaled dimerization dissociation constant $K_d = 1$ and Hill coefficient $n = 1.5$ (Box 1). In both (C) and (D), each axis represents the dimensionless total concentration of each transcription factor. Note that in the nondimensionalized model, changing protein stability is equivalent to multiplying α and β with the same factor (Box 1).

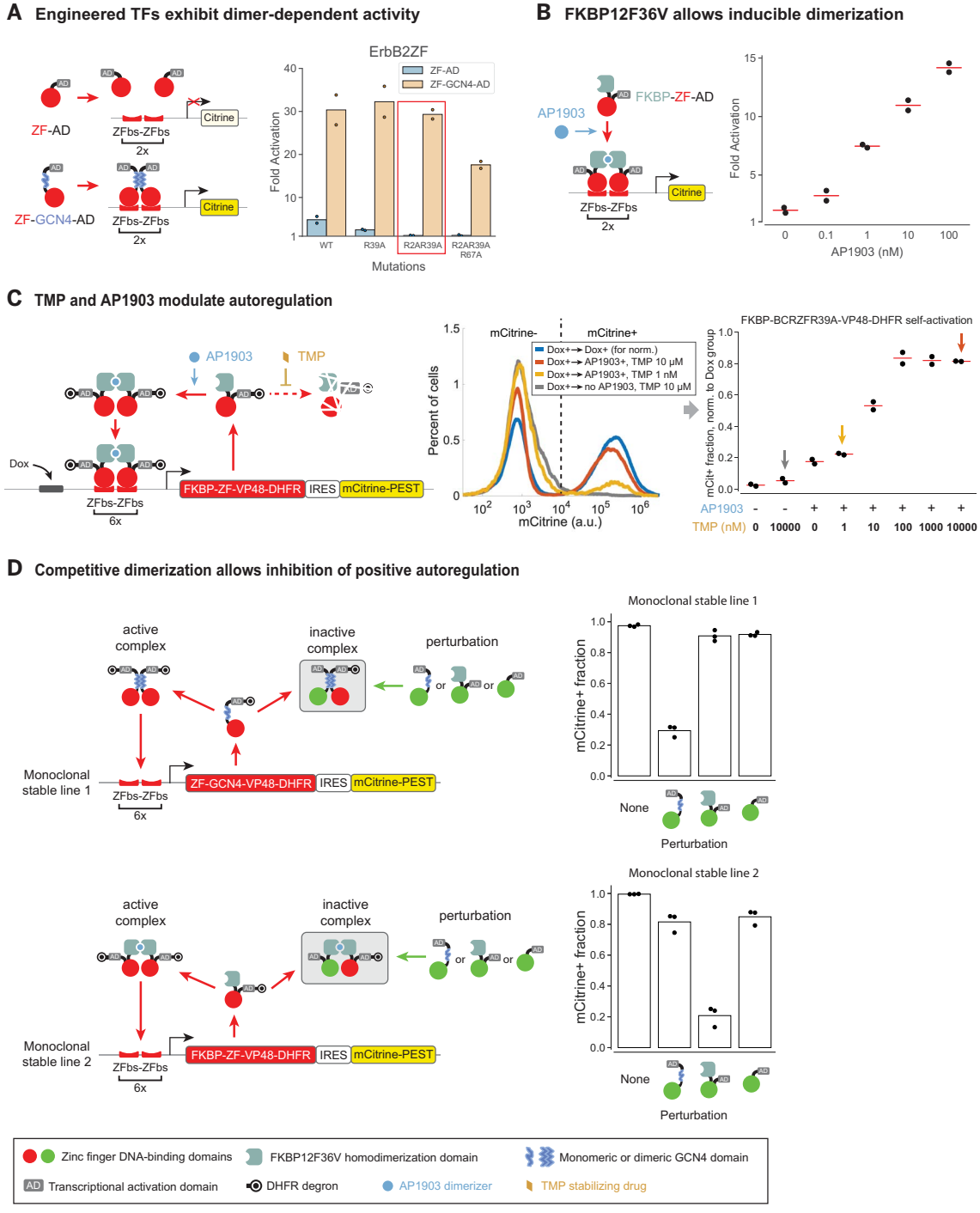

Fig. 2. Engineered transcription factors enable homodimer-dependent autoregulation and heterodimerization-based inhibition. (**A**) ZF transcription factors enable homodimer-dependent activation. Left: Design of test constructs in which ErbB2ZF (*31*) (red circle), fused to VP48 (AD) and in some cases GCN4 (blue squiggle) domains, binds to target sites (red pads) to activate Citrine expression. Activators were expressed from a constitutive CAG promoter (*52*). Right: R-to-A mutations in ZF-modulated reporter activation by ZF-GCN4-AD and ZF-AD. The R2AR39A variant was selected because of high ZF-GCN4-AD activation and minimal ZF-AD activation. Fold activation is defined in fig. S4A. WT, wild-type variant. (**B**) Left: Design of test constructs in which FKBP12F36V (FKBP, light cyan partial box), fused to BCRZFR39A (red circle) and VP48 (AD), binds to target sites (red pads) to activate Citrine expression in the presence of AP1903 (cyan circle). Right: This design allows dose-dependent control of activation by AP1903. (**C**) Transcription factor self-activation can be controlled by TMP and AP1903. Left: Design of the controllable self-activation circuit. IRES, internal ribosome entry site; PEST, constitutive degradation tag (*53*). Center: Stable polyclonal cells showed bimodal mCitrine distribution upon circuit activation. An empirical threshold at mCitrine = 10^4 separates the distribution into two fractions, and the normalized mCitrine$^+$ fraction was used to quantify the self-activation strength (*25*). Right: Colored arrows indicate data from the center panel. AP1903$^+$ samples had 100 nM AP1903. (**D**) Self-activation was inhibited by proteins with a different ZF and matching dimerization domains. Two monoclonal stable lines could spontaneously self-activate in media containing AP1903 and TMP (fig. S5B). Each perturbation construct is introduced by stable integration (*25*). The integrated construct in the "None" group did not express any perturbation protein. Red circle denotes 42ZFR2AR39AR67A; green circle denotes BCRZFR39A. In all panels, each dot represents one biological replicate, and each red line or bar indicates the mean of replicates. Lists of constructs and cell lines are in tables S2 and S3.

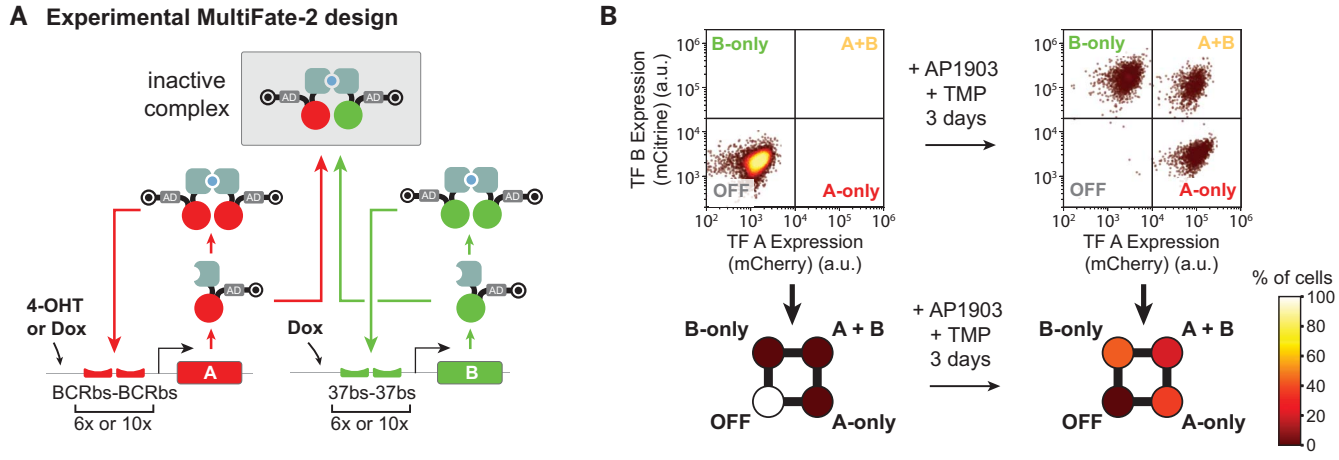

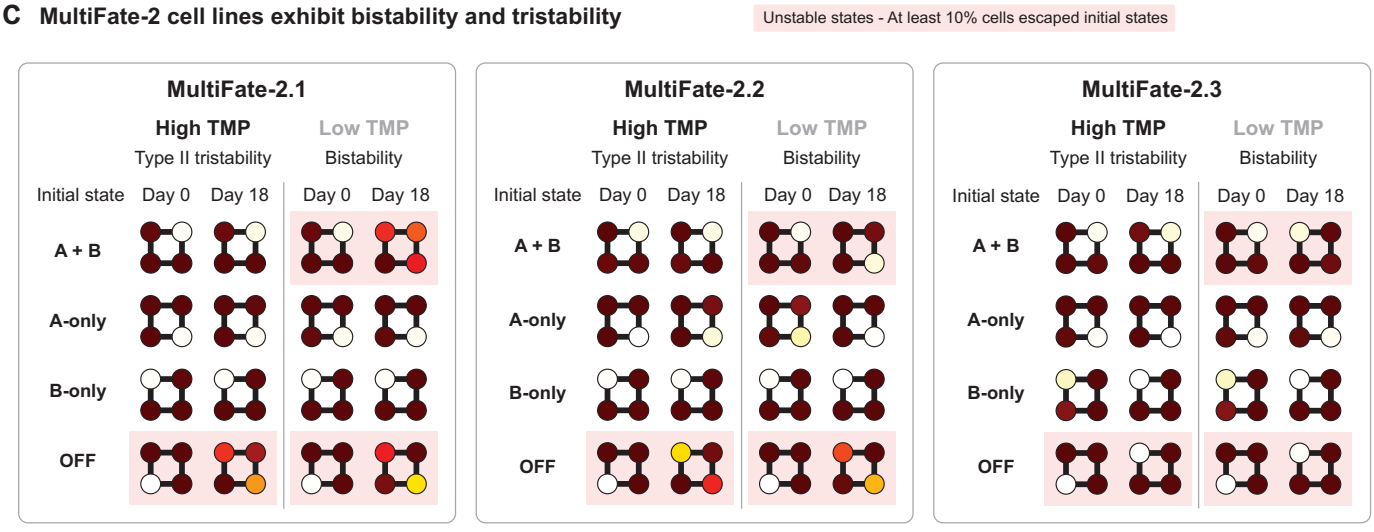

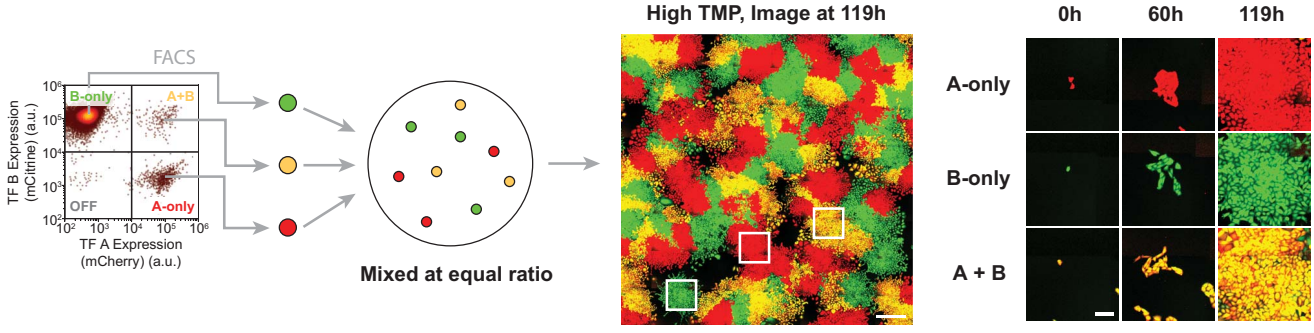

Fig. 3. MultiFate-2 generates multiple stable states. (**A**) The experimental MultiFate-2 design uses two self-activation cassettes differing only in their fluorescent proteins and their ZF DNA binding domains and binding sites. Each cassette expresses FKBP-ZF-VP16-DHFR-IRES-FP-PEST, where ZF represents either BCRZFR39A or 37ZFR2AR11AR39AR67A and FP represents either mCherry or mCitrine, for A and B, respectively. Detailed construct maps and differences among MultiFate-2 lines are shown in tables S2 and S3. (**B**) MultiFate-2.1 cells spontaneously activate A, B, or both cassettes upon addition of 100 nM AP1903 and 10 μM TMP. Cell percentages in OFF, A-only, B-only, and A+B states were quantified and plotted as a square with four colored circles (*31*); a.u., arbitrary units. (**C**) Three MultiFate-2 lines all exhibited type II tristability in the high-TMP condition and bistability in the low-TMP condition. In all conditions, we added 100 nM AP1903. Exact concentrations of TMP are shown in figs. S9 to S11. Unstable states, defined by states having more than 10% cells escaping their initial states after 18 days, were marked in pink rectangles. Each square represents the mean fractions of three biological replicates. Initial A-only, B-only, and A+B cells were sorted from a population of cells in different states, while initial OFF cells came from cells in regular CHO media without any inducers. (**D**) A-only, B-only, and A+B states were each stable during growth from single MultiFate-2.3 cells into colonies over 5 days (119 hours) under a time-lapse microscope. Left: We first sorted mixed MultiFate-2.3 cell populations to separate cells in three different states. Then we seeded cells in these three states at equal ratio in the same well and performed time-lapse imaging (*25*). Scale bars, 500 μm for the wide-field image, 100 μm for zoomed-in images. "High TMP" = 100 nM AP1903 + 10 μM TMP.

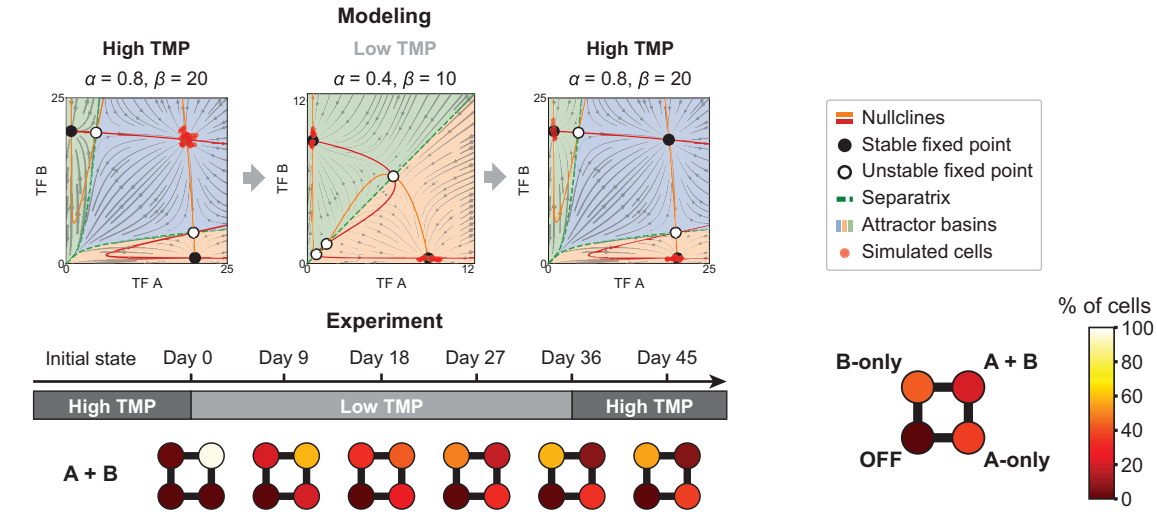

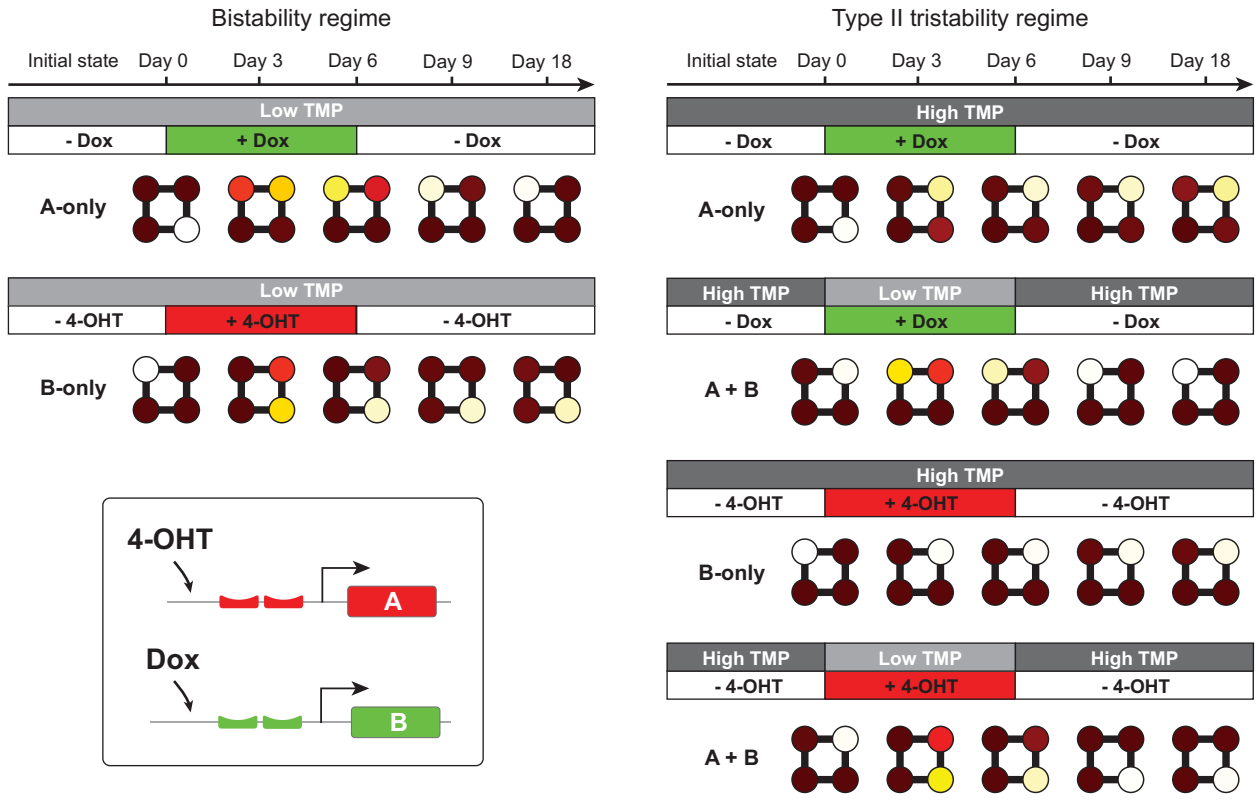

Fig. 4. MultiFate-2 supports modulation of state stability and allows state switching. (**A**) Escape from the destabilized A+B state was irreversible, as shown by both modeling and experiments that used MultiFate-2.1 cells. Top: The model used here is symmetric and nondimensionalized, with rescaled dimerization dissociation constant $K_d = 1$ and Hill coefficient $n = 1.5$ (Box 1). The x and y axes are total dimensionless concentrations of TF A and TF B, respectively. Simulated cells on phase portraits were calculated using the Gillespie algorithm (*25*, *54*). Note that in the nondimensionalized model, changing protein stability is equivalent to multiplying α and β with the same factor (Box 1). Bottom: Throughout the experiment, we added 100 nM AP1903. Exact concentrations of TMP are shown in fig. S9. (**B**) MultiFate-2.3 cells can be switched between states by transient 4-OHT (25 nM) or Dox (500 ng/ml) treatment. In all conditions, we added 100 nM AP1903. Exact concentrations of TMP are shown in fig. S16. In all panels, initial A-only, B-only, and A+B cells were sorted from a population of cells in different states. Each square represents the mean fractions of three biological replicates.

Box 1. Design of the MultiFate circuit.

Here we introduce the mathematical model of the MultiFate circuit and show how it can be used to design the experimental system and predict its behavior. For simplicity, we focus on a symmetric MultiFate-2 circuit whose two transcription factors share identical biochemical parameters and differ only in their DNA binding site specificity. A similar analysis of systems with more transcription factors and asymmetric parameters is presented in (*25*).

We represent the dynamics of protein production and degradation using ordinary differential equations (ODEs) for the total concentrations of the transcription factors A and B, denoted $[A_{tot}]$ and $[B_{tot}]$, respectively. We assume that the rate of production of each protein follows a Hill function of the corresponding homodimer concentration, $[A_2]$ or $[B_2]$, with maximal rate β, Hill coefficient n, and half-maximal activation at a homodimer concentration of K_M. A low basal protein production rate, denoted α, is included to allow self-activation from low initial expression states. Finally, each protein can degrade and be diluted (as a result of cell division) at a total rate δ, regardless of its dimerization state. To simplify analysis, we nondimensionalize the model by rescaling time in units of δ^{-1} and rescaling concentrations in units of K_M (*25*), and obtain

$$\frac{d[A_{tot}]}{dt} = \alpha + \frac{\beta[A_2]^n}{1+[A_2]^n} - [A_{tot}]$$
$$\frac{d[B_{tot}]}{dt} = \alpha + \frac{\beta[B_2]^n}{1+[B_2]^n} - [B_{tot}]$$

Here, Hill coefficient n only represents ultrasensitivity introduced by transcriptional activation. See (*25*) for a more detailed discussion on additional ultrasensitivity provided by homodimerization and molecular titration.

Because dimerization dynamics occur on a faster time scale than protein production and degradation (*49*), we assume that the distribution of monomer and dimer states remains close to their equilibrium values. This generates the following relationships between the concentrations of monomers, $[A]$ and $[B]$, and dimers, $[A_2]$, $[B_2]$, and $[AB]$:

$$[A]^2 = K_d[A_2]$$
$$[B]^2 = K_d[B_2]$$
$$2[A][B] = K_d[AB]$$

Because the two transcription factors share the same dimerization domain, homo- and heterodimerization are assumed to occur with equal dissociation constants K_d. Additionally, conservation of mass implies that $[A_{tot}] = [A] + [AB] + 2[A_2]$, with a similar relationship for B. Introducing the equilibrium equations given above into this conservation law produces expressions for the concentrations of the activating homodimers in terms of the total concentrations of A and B:

$$[A_2] = \frac{2[A_{tot}]^2}{K_d+4([A_{tot}]+[B_{tot}])+\sqrt{K_d^2+8([A_{tot}]+[B_{tot}])K_d}}$$
$$[B_2] = \frac{2[B_{tot}]^2}{K_d+4([A_{tot}]+[B_{tot}])+\sqrt{K_d^2+8([A_{tot}]+[B_{tot}])K_d}}$$

Inserting these expressions into the differential equations for $[A_{tot}]$ and $[B_{tot}]$ above, we obtain a pair of coupled ODEs with only $[A_{tot}]$ and $[B_{tot}]$ as variables.

To understand the behavior of this system in physiologically reasonable parameter regimes (table S1), we used standard approaches from dynamical systems analysis (*25*, *50*). We first generated a phase portrait of variables $[A_{tot}]$ and $[B_{tot}]$ based on ODEs (labeled "TF A" and "TF B," which are dimensionless total TF A or B concentrations), where the linewidth of a vector (Fig. 1C, gray arrows) at any point is proportional to the speed of that point. On the phase portrait, we plotted the nullclines (Fig. 1C, solid lines), defined by setting each of the ODEs above to zero. We then identified fixed points at nullcline intersections and determined their linear stability (Fig. 1C, black and white dots) (*50*). Finally, we delineated the basins of attraction for each stable fixed point (Fig. 1C, shaded regions).

Using this analysis, we identified parameter values that support type II tristability, a regime that minimally embodies the developmental concept of multilineage priming (*26*–*28*) (Fig. 1C and fig. S1B). Stronger self-activation (higher values of β) was more likely to produce type II tristability (fig. S1B, β row and column). Too much leaky production (high α) allowed both transcription factors to self-activate, reducing the degree of multistability, whereas too little (low α) stabilized the undesired OFF state (fig. S1B, α column). Strong dimerization (low K_d) was essential for type II tristability (fig. S1B, K_d row and column). Finally, a broad range of Hill coefficients $n \geq 1$ were compatible with type II tristability. Although higher values of n led to a reduced sensitivity to other parameters and allowed the system to tolerate higher values of α, they also stabilized the OFF state (fig. S1B, n row and column). Together, these results suggested that an ideal design would maximize β, minimize K_d, and use intermediate values of α and n.

On the basis of these conclusions, we incorporated multiple repeats of the homodimeric binding sites to maximize β, used strongly associating FKBP12F36V homodimerization domains (*36*) to minimize K_d, and modified the promoter sequences to allow some leaky expression to optimize α (fig. S24) (*25*). Finally, although we did not directly control n, we expected that the repeated homodimeric binding sites should lead to some ultrasensitivity (*51*). These design choices produced the selected type II tristability in the experimental system (Fig. 3C).

A key feature of the MultiFate design is its ability to qualitatively change its multistability properties through bifurcations in response to parameter changes. In particular, the mathematical model predicts that protein stability can control the number of stable fixed points in phase space. In the nondimensionalized model, the protein degradation rate, δ, does not appear explicitly but enters through the rescaling of α and β by $(\delta K_M)^{-1}$ (*25*). Thus, tuning protein stability is equivalent to multiplying both α and β by a common factor, which we term the "protein stability factor." Reducing protein stability shifts the nullclines closer to the origin, causing the two unstable fixed points to collide with the stable A+B fixed point in a subcritical pitchfork bifurcation (Fig. 1C) (*50*). The result is a bistable system with A-only and B-only stable fixed points at somewhat lower concentrations (Fig. 1C). To experimentally realize this bifurcation, we designed the circuit to allow external control of transcription factor protein stability using the drug-inducible DHFR degron (Fig. 2C) (*37*). As predicted, reducing protein stability destabilized the A+B state but preserved the A-only and B-only stable states (Fig. 3C). In this way, model-based design enabled us to rationally engineer tristability as well as externally controllable transitions to bistability in the experimental system.

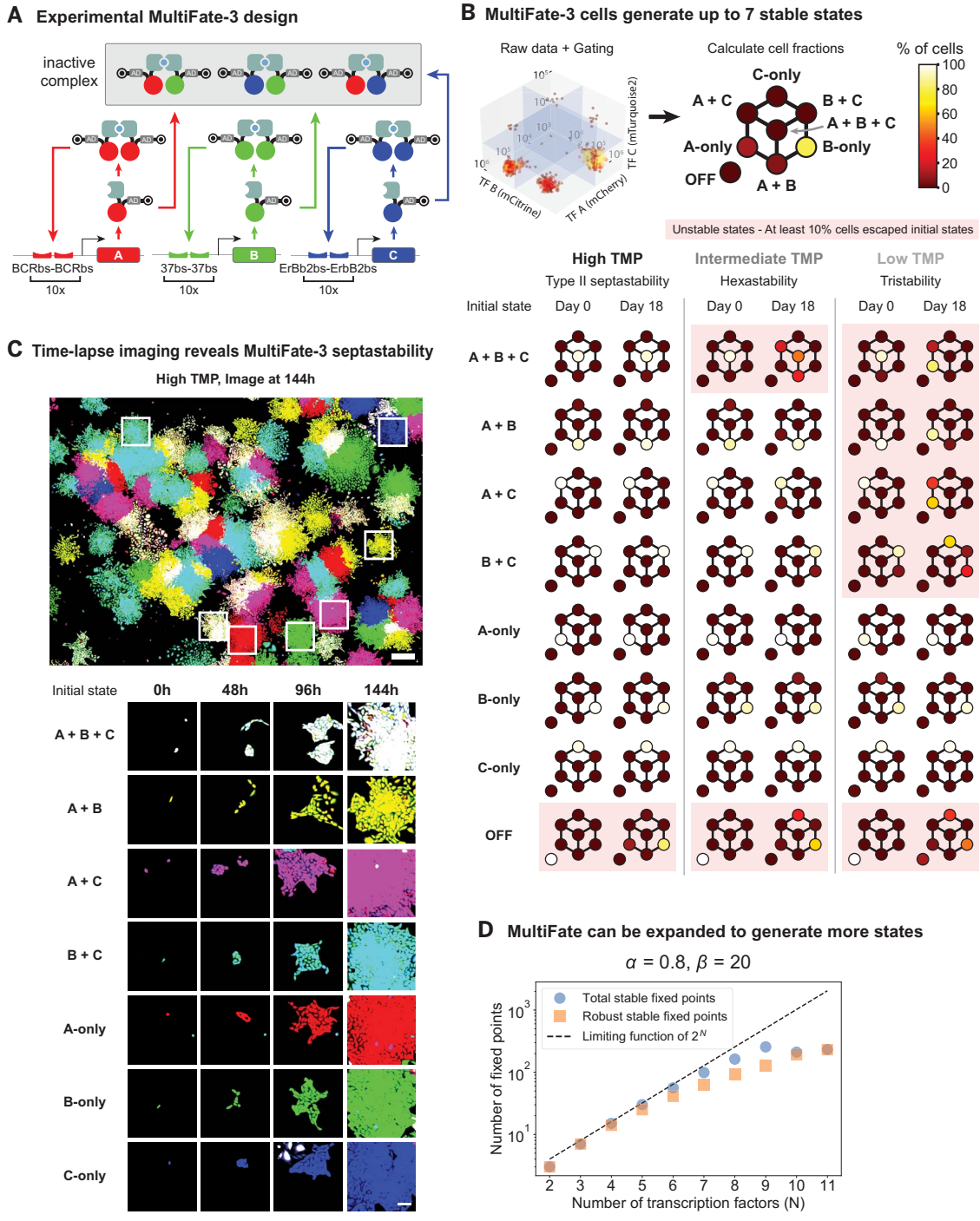

Fig. 5. MultiFate architecture is expandable to include three and potentially even more transcription factors. (**A**) The experimental MultiFate-3 design uses three self-activation cassettes differing only in their fluorescent proteins and their ZF DNA binding domains and binding sites. Each cassette expresses FKBP-ZF-VP16-DHFR-IRES-FP-PEST, where ZF represents either BCRZFR39A, 37ZFR2AR11-AR39AR67A, or ErbB2ZFR2AR39A and FP represents either mCherry, mCitrine, or mTurquoise2 for A, B, and C, respectively. See table S2 for detailed construct maps. (**B**) The MultiFate-3 line exhibited type II septastability, hexastability, and tristability in three different TMP conditions. Top: State percentages in each octant were quantified and plotted as eight colored circles (*25*). Bottom: High-TMP condition = 100 nM AP1903 + 100 nM TMP; intermediate-TMP condition = 100 nM AP1903 + 40 nM TMP; low-TMP condition = 100 nM AP1903 + 10 nM TMP. Except for OFF-state cells, cells in different initial states were sorted from a mixed population of cells in the high-TMP condition. Initial OFF cells came from cells in regular CHO media without any inducers. Each plot represents the mean percentage of three biological replicates. (**C**) Cells in each of the seven states were stable during growth from single cells into colonies over 6 days under a time-lapse microscope. We sorted cells and seeded an equal ratio of cells in seven states using the same method as in Fig. 3D. Scale bars, 500 μm for the wide-field image, 100 μm for zoomed-in images. (**D**) MultiFate is expandable. The number of robust stable fixed points grows monotonically with the number of transcription factor species (*N*) in the model. A robust stable fixed point is defined as a stable fixed point that has fewer than 10% of cells escaping at the end of stochastic simulations (*25*). The parameter set provided above the plot (with K_d = 1 and n = 1.5) is the same nondimensionalized parameter set used in MultiFate-2 and MultiFate-3 models under high protein stability.

marker, into Chinese hamster ovary K1 (CHO-K1) cells and analyzed Citrine expression by flow cytometry 36 hours later (Fig. 2A and fig. S4A) (*25*). The wild-type (WT) ZF-GCN4-AD factors strongly activated the reporter, as desired, whereas ZF-AD exhibited weaker, but still undesirable, basal activity (Fig. 2A and fig. S4B). Following previous work (*29*, *34*, *35*), we incorporated arginine-to-alanine mutations at key positions in the ZF known to weaken DNA binding, which decreased monomeric activity without reducing homodimer activity (Fig. 2A, red square). Replacing the GCN4 with the FKBP12F36V (FKBP) homodimerization domain (*36*) allowed us to achieve dose-dependent control of dimerization with the small molecule AP1903 (Fig. 2B). Finally, we repeated this general design to engineer a set of additional homodimer-dependent ZF transcription factors with orthogonal DNA binding specificities (fig. S4, B and C).

The MultiFate circuit design requires that each transcription factor positively autoregulates its own expression in a homodimer-dependent manner. To validate this capability, we designed a self-activation construct (Fig. 2C, left) in which a transcription factor with an FKBP dimerization domain is expressed from a promoter containing its own 18-bp homodimer binding sites (table S2). This construct allowed independent doxycycline (Dox)–inducible activation through upstream Tet3G (Takara Bio) binding sites. It also incorporated a dihydrofolate reductase (DHFR) degron (*37*), which can be inhibited by trimethoprim (TMP), permitting control of protein stability. Finally, we incorporated a destabilized mCitrine for dynamic readout of construct expression. We integrated this construct into Tet3G-expressing CHO-K1 cells, generating a stable polyclonal population for further analysis (table S3) (*25*).

To test for self-activation, we transiently induced transcription factor expression for 24 hours with Dox, and then withdrew Dox and checked whether cells could sustain circuit activation when dimerization strength and protein stability were varied by AP1903 and TMP, respectively. In the presence, but not the absence, of AP1903, cells exhibited a bimodal distribution of mCitrine fluorescence, with well-separated peaks (Fig. 2C, center), consistent with homodimer-dependent self-activation in a subset of cells. TMP, by stabilizing transcription factors, also promoted self-activation in a dose-dependent manner (Fig. 2C and fig. S5A). Thus, a single dimer-dependent transcription factor can self-activate and sustain its own expression in a controllable manner.

MultiFate's final requirement is the ability of one transcription factor to effectively inhibit another through heterodimerization. To test this, we selected monoclonal cell lines with the self-activating circuits, and then stably integrated constructs expressing proteins with a different ZF DNA binding domain and a matching or mismatching dimerization domain to generate a polyclonal cell population for each perturbation construct (tables S2 and S3) (*25*). Consistent with inhibition through heterodimerization, the proteins with matching dimerization domains strongly inhibited the self-activating transcription factor, whereas similar proteins with nonmatching dimerization domains exhibited much weaker inhibition, possibly through nonspecific mechanisms (Fig. 2D and fig. S5B). Taken together, these results provided a set of engineered ZF transcription factors that exhibited controllable homodimer-dependent activation and heterodimer-dependent inhibition.

The MultiFate-2 circuit generates tristability

To construct a complete MultiFate circuit, we selected two dimer-dependent transcription factors, designated A and B, with distinct DNA binding specificities but the same FKBP homodimerization domain. Their expressions were driven by promoters containing multiple repeats of their corresponding 18-bp homodimer binding sites (Fig. 3A and table S2). The promoters also incorporated Tet3G or ERT2-Gal4 response elements (*38*) to allow independent external activation of transcription. Factors A and B were transcriptionally coexpressed with destabilized mCherry or mCitrine fluorescent proteins, respectively, each placed after an internal ribosome entry site (IRES), allowing fluorescent readout of transcription rates in individual cells (fig. S6). We stably integrated both genes simultaneously in CHO-K1 cells expressing Tet3G and ERT2-Gal4 proteins, and then selected and further characterized three stable monoclonal cell lines, designated MultiFate-2.1, MultiFate-2.2, and MultiFate-2.3, with different promoter configurations (fig. S7A and table S3) (*25*).

To test whether MultiFate circuits support multistability, we activated the circuit by transferring MultiFate-2.1 cells to media containing AP1903 and TMP to allow dimerization and stabilizing the transcription factors. As expected in the regime of type II tristability (Fig. 1C), cells went from low expression of both transcription factors (OFF state) to one of three distinct states, with either A, B, or both transcription factors highly expressed (Fig. 3B). We designated these states A-only, B-only, and A+B, respectively. The three states were well separated by differences in either mCherry or mCitrine expression by a factor of ~25 to 50, and cells grew at similar rates among states (fig. S8). To assess their stability, we sorted cells from each of these states and cultured them continuously for 18 days (*25*). Strikingly, nearly all cells remained in the sorted state for this extended period (Fig. 3C, MultiFate-2.1 high-TMP columns, and fig. S9), despite gene expression noise (observable from the spread of cellular fluorescence on flow cytometry plots). This showed that cells were attracted to these states. Stability required positive autoregulation, as withdrawal of AP1903 and TMP collapsed the expression of both factors within 2 days (fig. S9). Similar overall behavior was also observed in MultiFate-2.2 and MultiFate-2.3 (Fig. 3C and figs. S10 and S11). All three MultiFate-2 cell lines thus exhibited dynamics consistent with type II tristability (Fig. 1C).

Time-lapse imaging provided a more direct view of multistability. We cultured an equal ratio of single cells sorted from three different initial states in the same well and imaged them as they developed into colonies (Fig. 3D) (*25*). In almost all colonies (132 of 134), all cells maintained their initial states for the full duration of the movie, at least 5 days or seven to eight cell cycles (Fig. 3D, figs. S12A and S13A, and movie S2). Together with the flow cytometry analysis, these results demonstrate that all three MultiFate-2 lines can sustain long-term tristability.

MultiFate-2 supports modulation of state stability and allows controlled state switching

The ability of a transient stimulus to destabilize multipotent states and trigger an irreversible fate change is a hallmark of many cell fate control systems (*12*–*14*). In the model, reducing protein stability can eliminate the A+B state while preserving the A-only and B-only states (Fig. 1C). As a result, cells initially occupying the A+B state transition to A-only or B-only states (Fig. 4A, top). When protein stability is restored to its initial value, the A+B attractor reappears. However, for the parameter sets analyzed here, cells remain within the attractor basins of A-only and B-only states and therefore do not return to the A+B state (Fig. 4A, top). Stochastic simulations of single-cell dynamics confirmed this irreversible (hysteretic) behavior (Fig. 4A, top, and movie S3).

To test whether similar bifurcation and hysteretic dynamics occur in the experimental system, we transferred A-only, B-only, and A+B cells from media containing high TMP concentrations ("high TMP") to similar media with reduced TMP concentrations ("low TMP"), which decreased protein stability by permitting degron function. As predicted, reducing protein stability selectively destabilized the A+B state, but not the A-only and B-only states, shifting cells from the A+B state to the A-only or B-only states (Fig. 3C, low-TMP columns, and Fig. 4A, bottom). Different MultiFate-2 cell lines exhibited different transition biases, reflecting clone-specific asymmetries in the experimental MultiFate-2 systems (Fig. 3C and figs. S9 to S11), in a manner consistent with an asymmetric MultiFate model (movie S3 and figs. S14 and S15) (*25*). Escape from the destabilized A+B state was irreversible, as cells remained in the A-only or B-only state even after they were

transferred back to the high-TMP media (Fig. 4A, bottom, and fig. S9). Thus, MultiFate's ability to support irreversible transitions allows it to produce behaviors resembling stem cell differentiation.

Finally, we asked to what extent we could deliberately switch cells from one state to another through transient perturbations. We used MultiFate-2.3, in which the A and B genes can be independently activated by 4-hydroxy-tamoxifen (4-OHT) and Dox, respectively, to address this question. In this line, the response elements for the inducers are adjacent to the homodimer binding sites. Therefore, the addition of inducers increases A or B expression up to, but not substantially beyond, the level produced by self-activation (Fig. 2C and fig. S16). In the bistable regime, transient induction of either transcription factor switched cells into the corresponding state, where they remained in the absence of further induction (Fig. 4B, left, and figs. S3A and S16A). In the tristable regime, the model predicted, and experiments confirmed, that transient induction of B by Dox could switch A-only cells to the A+B state, but not beyond it to the B-only state (Fig. 4B, top right; fig. S3B, first row; and fig. S16B). Combining transient Dox addition to induce B expression with TMP reduction to destabilize the A+B state successfully transitioned cells from the A+B to the B-only state (Fig. 4B, right second row, and fig. S3B, second row). The reciprocal experiments, in which we induced A expression with 4-OHT with or without reduced TMP, produced equivalent results (Fig. 4B, right column, lower two rows). Taken together, these results demonstrate that MultiFate-2 circuits allow modulation of state stability, irreversible cell state transitions, and direct control of state switching with transient external inducers.

MultiFate is expandable

Because the MultiFate system implements mutual inhibition among transcription factors through heterodimerization, it can be expanded by adding additional transcription factors without reengineering existing components. In the model, adding a third transcription factor to a MultiFate-2 circuit produces a range of new stability regimes containing three, four, six, seven, or eight stable fixed points, depending on parameter values (Fig. 1D, fig. S2, and movie S4) (*25*). To test whether experimental MultiFate-2 circuits can be similarly expanded, we stably integrated a third ZF transcription factor, denoted C, containing the same FKBP dimerization domain as A and B, coexpressed with a third fluorescent protein, mTurqoise2, into the MultiFate-2.2 cell line to obtain the MultiFate-3 cell line (Fig. 5A, fig. S7B, and table S3) (*25*).

After the addition of AP1903 and TMP, MultiFate-3 cells went from low expression of all genes (OFF state) to one of seven distinct expression states, termed A-only, B-only, C-only, A+B, A+C, B+C, and A+B+C states (Fig. 5B), consistent with a type II septastability regime (Fig. 1D and fig. S2A). Most cells occupied the B-only state (79.5 ± 0.3%), reflecting asymmetries within the circuit (figs. S14 and S15). To assess the stability of these states, we sorted cells from each of the seven states and continuously cultured them in media containing AP1903 and TMP, analyzing the culture every 3 days by flow cytometry (*25*). Remarkably, each of the seven states was stable for the full 18-day duration of the experiment (Fig. 5B, high-TMP columns, and fig. S17). Long-term stability required AP1903 and TMP, as expected (fig. S18). Finally, cells from each state could be reset by withdrawal of AP1903 and TMP and then redifferentiated into all seven states when AP1903 and TMP were added back (fig. S18). This indicates that the observed stability is not the result of a mixture of clones permanently locked into distinct expression states.

To directly visualize the septastable dynamics of MultiFate-3, we cocultured single cells sorted from each of the seven states and performed live imaging as they grew into colonies (*25*). Consistent with the flow cytometry results, cells retained their initial states for the full 6-day duration of the experiment in almost every colony (153 of 157) (Fig. 5C, figs. S12B and S13B, and movie S5).

Like MultiFate-2, the number and stability of different states in MultiFate-3 can be modulated. In the model, reducing protein stability repeatedly bifurcates the system from type II septastability (seven stable states) through hexastability (six stable states) to tristability (three stable states) (Fig. 1D). This process resembles the progressive loss of cell fate potential during stem cell differentiation (*39*). To experimentally test this prediction, we transferred cells in each of the seven states cultured under the high-TMP (100 nM) condition (high protein stability) to similar media with intermediate-TMP (40 nM) or low-TMP (10 nM) conditions. As predicted by the model, the intermediate-TMP condition destabilized only the A+B+C state, but not the other six states (Fig. 5B, intermediate-TMP columns, and fig. S19), whereas the low-TMP condition destabilized all multiprotein states, preserving only the A-only, B-only, and C-only states (Fig. 5B, low-TMP columns, and fig. S20). Consistent with the model, these transitions were also irreversible: Restoring high TMP concentrations did not cause cells to repopulate previously destabilized states (fig. S21 and movie S6). Taken together, these results demonstrate that the MultiFate-3 circuit supports septastability and allows controlled bifurcations to produce irreversible cell state transitions.

Can the MultiFate architecture be expanded beyond three transcription factors? To understand higher-order systems, we modeled MultiFate circuits containing up to $N = 11$ transcription factors (*25*). Using the same parameter values established for MultiFate-2 and MultiFate-3, the number of attractors reached a maximum of 256 at $N = 9$. Analysis of attractor escape rates in stochastic simulations revealed that most of these attractors were robust to gene expression noise (Fig. 5D and fig. S22) (*25*, *40*). The number of attractors grew more slowly than the theoretical limit of $\sim 2^N$ because stable attractors could only sustain high levels of up to four transcription factors at a time (fig. S23, middle row). This limitation reflects the diminishing share of the active homodimers relative to all dimers. Similarly, the combined basal expression of all transcription factors suppressed homodimer formation, resulting in a decline in the number of attractors for systems containing more than nine transcription factors (Fig. 5D and fig. S23, middle row). Finally, we note that the precise values of the maximum number of stable attractors can be modulated up or down by parameters that affect overall gene expression (fig. S23). Together, these results indicate that the MultiFate architecture can be expanded to generate large numbers of robust stable states.

Discussion

The astonishing diversity of cell types in our own bodies underscores the critical importance of multistable circuits and provokes the fundamental question of how to engineer a robust, controllable, and expandable synthetic multistable system. We took inspiration from two ubiquitous features of natural multistable systems, namely competitive protein-protein interactions and transcriptional autoregulation, to design a synthetic multistable architecture that operates in mammalian cells. The MultiFate circuits exhibit many of the hallmarks of natural cell fate control systems. They generate as many as seven molecularly distinct, mitotically heritable cell states (Figs. 3 and 5). They allow controlled switching of cells between states with transient transcription factor expression (Fig. 4B), similar to fate reprogramming (*16*). They support modulation of state stability (Figs. 3 and 5) and permit irreversible cellular transitions through externally controllable parameters such as protein stability (Fig. 4A and fig. S21), similar to the irreversible loss of cell fate potential during stem cell differentiation (*12*). Finally, implementing cross-inhibition at the protein level makes MultiFate expandable by "plugging in" additional transcription factors without reengineering the existing circuit, a useful feature for synthetic biology. The same design principle may play a related role in natural systems, allowing the emergence of new cell states through transcription factor duplication and subfunctionalization

in a manner analogous to the stepwise expansion of MultiFate circuits demonstrated here (*21*, *22*, *41*, *42*).

A remarkable feature of this circuit is its close agreement with predictions from a dynamical systems model (Box 1). Despite a lack of precise quantitative parameter values for many molecular interactions, the qualitative behaviors possible with this circuit design can be enumerated and explained from simple properties of the components and their interactions. More precise measurements of effective biochemical parameters and stochastic fluctuations could help to explain, eliminate, or exploit asymmetries and provide a better understanding of the time scales of state transitions.

MultiFate has a relatively simple structure, requiring a small number of genes, all of the same type, yet exhibits robust memory behaviors, scalability, and predictive design. Future work should extend MultiFate into a full-fledged synthetic cell fate control system. Coupling MultiFate to synthetic cell-cell communication systems such as synNotch (*43*, *44*), MESA (*45*), synthekines (*46*), engineered GFP (*47*), and auxin (*48*) should enable navigation of cells through a series of fate choices, recapitulating cell behaviors associated with normal development. MultiFate could also allow engineering of multicellular cell therapeutic programs. For example, one could engineer a stemlike state that can either self-renew or "differentiate" into other states that recognize and remember different input signals and communicate with one another to coordinate complex response programs. Such strategies will benefit from the ability of MultiFate to allow probabilistic differentiation into multiple different states in the same condition (fig. S14). In this way, we anticipate that the MultiFate architecture will provide a scalable foundation for exploring the circuit-level principles of cell fate control and will enable new multicellular applications in synthetic biology.

Methods summary

We performed all tissue culture experiments with CHO-K1 cells (ATCC). For flow cytometry experiments characterizing ZF transcription factors (Fig. 2, A and B, and fig. S4), we cotransfected CHO-K1 cells with mTagBFP2 (as cotransfection marker), reporter, and ZF transcription factor (table S2). Cells were harvested after 36 hours and cell fluorescence was measured by flow cytometry. For experiments characterizing ZF transcription factor self-activation (Fig. 2C and fig. S5A), we stably integrated each self-activation construct (table S2) into polyclonal Tet3G-expressing CHO-K1 cells via PiggyBac (Systems Biosciences) to make a polyclonal cell line (table S3). We transiently activated the integrated self-activation cassettes in each polyclonal line by adding Dox (Sigma-Aldrich) for 24 hours, then washed out Dox and transferred cells into different combinations of AP1903 and/or TMP (Sigma-Aldrich). After another 72 hours, cells were harvested and analyzed by flow cytometry. To test inhibition through competitive dimerization (Fig. 2D and fig. S5B), we selected two monoclonal self-activation lines with 42ZFR2AR39AR67A DNA binding domain and either GCN4 or FKBP dimerization domain. We stably integrated plasmids constitutively expressing different perturbation transcription factors in each monoclonal line, then transferred cells in media containing AP1903 and TMP to permit self-activation. The inhibition strength was quantified as the reduction of self-activation cell fractions.

We constructed MultiFate-2 lines by stably integrating corresponding constructs into polyclonal ERT2-Gal4-P2A-Tet3G–expressing CHO-K1 cells (table S3). We then used fluorescence-activated cell sorting to sort stable A+B cells in media containing AP1903 and TMP as single cells into 384-well plates to obtain monoclonal MultiFate-2 lines. We constructed MultiFate-3 cells by stably integrating the TF C self-activation cassette into MultiFate-2.2 cells, then used a similar sorting method to obtain the MultiFate-3 monoclonal cells (fig. S7).

For flow cytometry experiments characterizing state stability (Figs. 3C and 5B) and state-switching dynamics (Fig. 4), we sorted cells from each state into media containing the corresponding inducers. We continuously cultured these cells by trypsinizing cells and transferred 4% of cells into fresh media containing corresponding inducers every 3 days. The remaining 96% of cells were suspended in the flow cytometry buffer and analyzed by flow cytometry. For time-lapse imaging (Fig. 3D, Fig. 5C, and movies S2 and S5), we sorted cells from each state, mixed them with equal ratio, and sparsely plated cell mixture in the same well with media containing AP1903 and TMP. After 6 to 12 hours, we changed media and began imaging.

Mathematical models of MultiFate circuits are summarized in Box 1 and supplementary text (*25*). All data, computational and analysis codes, and sequence files are available at data.caltech.edu/records/1882. Full materials and methods are available in (*25*).

REFERENCES AND NOTES

1. S. Ramón y Cajal, *Histology of the Nervous System of Man and Vertebrates* (Oxford Univ. Press, 1995).
2. S. Huang, Multistability and Multicellularity: Cell Fates as High-Dimensional Attractors of Gene Regulatory Networks. *Comput. Syst. Biol.* **2006**, 293–326 (2006). doi: 10.1016/B978-012088786-6/50033-2
3. T. S. Gardner, C. R. Cantor, J. J. Collins, Construction of a genetic toggle switch in Escherichia coli. *Nature* **403**, 339–342 (2000). doi: 10.1038/35002131; pmid: 10659857
4. C. M. Ajo-Franklin *et al.*, Rational design of memory in eukaryotic cells. *Genes Dev.* **21**, 2271–2276 (2007). doi: 10.1101/gad.1586107; pmid: 17875664
5. B. P. Kramer *et al.*, An engineered epigenetic transgene switch in mammalian cells. *Nat. Biotechnol.* **22**, 867–870 (2004). doi: 10.1038/nbt980; pmid: 15184906
6. T. Lebar *et al.*, A bistable genetic switch based on designable DNA-binding domains. *Nat. Commun.* **5**, 5007 (2014). doi: 10.1038/ncomms6007; pmid: 25264186
7. D. R. Burrill, M. C. Inniss, P. M. Boyle, P. A. Silver, Synthetic memory circuits for tracking human cell fate. *Genes Dev.* **26**, 1486–1497 (2012). doi: 10.1101/gad.189035.112; pmid: 22751502
8. J. Santos-Moreno, E. Tasiudi, J. Stelling, Y. Schaerli, Multistable and dynamic CRISPRi-based synthetic circuits. *Nat. Commun.* **11**, 2746 (2020). doi: 10.1038/s41467-020-16574-1; pmid: 32488086
9. F. Wu, R.-Q. Su, Y.-C. Lai, X. Wang, Engineering of a synthetic quadrastable gene network to approach Waddington landscape and cell fate determination. *eLife* **6**, e23702 (2017). doi: 10.7554/eLife.23702; pmid: 28397688
10. H. Y. Kueh, A. Champhekar, S. L. Nutt, M. B. Elowitz, E. V. Rothenberg, Positive feedback between PU.1 and the cell cycle controls myeloid differentiation. *Science* **341**, 670–673 (2013). doi: 10.1126/science.1240831; pmid: 23868921
11. G. Yao, T. J. Lee, S. Mori, J. R. Nevins, L. You, A bistable Rb-E2F switch underlies the restriction point. *Nat. Cell Biol.* **10**, 476–482 (2008). doi: 10.1038/ncb1711; pmid: 18364697
12. S. Huang, Y.-P. Guo, G. May, T. Enver, Bifurcation dynamics in lineage-commitment in bipotent progenitor cells. *Dev. Biol.* **305**, 695–713 (2007). doi: 10.1016/j.ydbio.2007.02.036; pmid: 17412320
13. W. Xiong, J. E. Ferrell Jr., A positive-feedback-based bistable 'memory module' that governs a cell fate decision. *Nature* **426**, 460–465 (2003). doi: 10.1038/nature02089; pmid: 14647386
14. A. Gunne-Braden *et al.*, GATA3 Mediates a Fast, Irreversible Commitment to BMP4-Driven Differentiation in Human Embryonic Stem Cells. *Cell Stem Cell* **26**, 693–706.e9 (2020). doi: 10.1016/j.stem.2020.03.005; pmid: 32302522
15. K. M. Loh *et al.*, Mapping the Pairwise Choices Leading from Pluripotency to Human Bone, Heart, and Other Mesoderm Cell Types. *Cell* **166**, 451–467 (2016). doi: 10.1016/j.cell.2016.06.011; pmid: 27419872
16. K. Takahashi, S. Yamanaka, Induction of pluripotent stem cells from mouse embryonic and adult fibroblast cultures by defined factors. *Cell* **126**, 663–676 (2006). doi: 10.1016/j.cell.2006.07.024; pmid: 16904174
17. D. Arendt *et al.*, The origin and evolution of cell types. *Nat. Rev. Genet.* **17**, 744–757 (2016). doi: 10.1038/nrg.2016.127; pmid: 27818507
18. C. Sokolik *et al.*, Transcription factor competition allows embryonic stem cells to distinguish authentic signals from noise. *Cell Syst.* **1**, 117–129 (2015). doi: 10.1016/j.cels.2015.08.001; pmid: 26405695
19. A. Bhattacharya, N. E. Baker, A network of broadly expressed HLH genes regulates tissue-specific cell fates. *Cell* **147**, 881–892 (2011). doi: 10.1016/j.cell.2011.08.055; pmid: 22078884
20. H. Hosokawa *et al.*, Transcription Factor PU.1 Represses and Activates Gene Expression in Early T Cells by Redirecting Partner Transcription Factor Binding. *Immunity* **48**, 1119–1134.e7 (2018). doi: 10.1016/j.immuni.2018.04.024; pmid: 29924977
21. S. Stefanovic *et al.*, Interplay of Oct4 with Sox2 and Sox17: A molecular switch from stem cell pluripotency to specifying a cardiac fate. *J. Cell Biol.* **186**, 665–673 (2009). doi: 10.1083/jcb.200901040; pmid: 19736317
22. I. Aksoy *et al.*, Oct4 switches partnering from Sox2 to Sox17 to reinterpret the enhancer code and specify endoderm. *EMBO J.* **32**, 938–953 (2013). doi: 10.1038/emboj.2013.31; pmid: 23474895
23. M. J. Thayer *et al.*, Positive autoregulation of the myogenic determination gene MyoD1. *Cell* **58**, 241–248 (1989). doi: 10.1016/0092-8674(89)90838-6; pmid: 2546677
24. L. A. Neuhold, B. Wold, HLH forced dimers: Tethering MyoD to E47 generates a dominant positive myogenic factor insulated from negative regulation by Id. *Cell* **74**, 1033–1042 (1993). doi: 10.1016/0092-8674(93)90725-6; pmid: 7691411
25. See supplementary materials.
26. S. Bessonnard *et al.*, Gata6, Nanog and Erk signaling control cell fate in the inner cell mass through a tristable regulatory network. *Development* **141**, 3637–3648 (2014). doi: 10.1242/dev.109678; pmid: 25209243
27. P. Laslo *et al.*, Multilineage transcriptional priming and determination of alternate hematopoietic cell fates. *Cell* **126**,

755–766 (2006). doi: 10.1016/j.cell.2006.06.052; pmid: 16923394
28. T. Miyamoto *et al*., Myeloid or lymphoid promiscuity as a critical step in hematopoietic lineage commitment. *Dev. Cell* **3**, 137–147 (2002). doi: 10.1016/S1534-5807(02)00201-0; pmid: 12110174
29. A. S. Khalil *et al*., A synthetic biology framework for programming eukaryotic transcription functions. *Cell* **150**, 647–658 (2012). doi: 10.1016/j.cell.2012.05.045; pmid: 22863014
30. R. R. Beerli, D. J. Segal, B. Dreier, C. F. Barbas 3rd, Toward controlling gene expression at will: Specific regulation of the erbB-2/HER-2 promoter by using polydactyl zinc finger proteins constructed from modular building blocks. *Proc. Natl. Acad. Sci. U.S.A.* **95**, 14628–14633 (1998). doi: 10.1073/pnas.95.25.14628; pmid: 9843940
31. J. J. Lohmueller, T. Z. Armel, P. A. Silver, A tunable zinc finger-based framework for Boolean logic computation in mammalian cells. *Nucleic Acids Res.* **40**, 5180–5187 (2012). doi: 10.1093/nar/gks142; pmid: 22323524
32. C. J. Bashor *et al*., Complex signal processing in synthetic gene circuits using cooperative regulatory assemblies. *Science* **364**, 593–597 (2019). doi: 10.1126/science.aau8287; pmid: 31000590
33. O. M. Subach, P. J. Cranfill, M. W. Davidson, V. V. Verkhusha, An enhanced monomeric blue fluorescent protein with the high chemical stability of the chromophore. *PLOS ONE* **6**, e28674 (2011). doi: 10.1371/journal.pone.0028674; pmid: 22174863
34. P. S. Donahue *et al*., The COMET toolkit for composing customizable genetic programs in mammalian cells. *Nat. Commun.* **11**, 779 (2020). doi: 10.1038/s41467-019-14147-5; pmid: 32034124
35. M. Elrod-Erickson, T. E. Benson, C. O. Pabo, High-resolution structures of variant Zif268-DNA complexes: Implications for understanding zinc finger-DNA recognition. *Structure* **6**, 451–464 (1998). doi: 10.1016/S0969-2126(98)00047-1; pmid: 9562555
36. T. Clackson *et al*., Redesigning an FKBP-ligand interface to generate chemical dimerizers with novel specificity. *Proc. Natl. Acad. Sci. U.S.A.* **95**, 10437–10442 (1998). doi: 10.1073/pnas.95.18.10437; pmid: 9724721
37. M. Iwamoto, T. Björklund, C. Lundberg, D. Kirik, T. J. Wandless, A general chemical method to regulate protein stability in the mammalian central nervous system. *Chem. Biol.* **17**, 981–988 (2010). doi: 10.1016/j.chembiol.2010.07.009; pmid: 20851347
38. S. S. Gerety *et al*., An inducible transgene expression system for zebrafish and chick. *Development* **140**, 2235–2243 (2013). doi: 10.1242/dev.091520; pmid: 23633515
39. F. Notta *et al*., Distinct routes of lineage development reshape the human blood hierarchy across ontogeny. *Science* **351**, aab2116 (2016). doi: 10.1126/science.aab2116; pmid: 26541609
40. P. S. Swain, M. B. Elowitz, E. D. Siggia, Intrinsic and extrinsic contributions to stochasticity in gene expression. *Proc. Natl. Acad. Sci. U.S.A.* **99**, 12795–12800 (2002). doi: 10.1073/pnas.162041399; pmid: 12237400
41. K. Pougach *et al*., Duplication of a promiscuous transcription factor drives the emergence of a new regulatory network. *Nat. Commun.* **5**, 4868 (2014). doi: 10.1038/ncomms5868; pmid: 25204769
42. J. González *et al*., Diversification of Transcriptional Regulation Determines Subfunctionalization of Paralogous Branched Chain Aminotransferases in the Yeast *Saccharomyces cerevisiae*. *Genetics* **207**, 975–991 (2017). doi: 10.1534/genetics.117.300290; pmid: 28912343
43. L. Morsut *et al*., Engineering Customized Cell Sensing and Response Behaviors Using Synthetic Notch Receptors. *Cell* **164**, 780–791 (2016). doi: 10.1016/j.cell.2016.01.012; pmid: 26830878
44. S. Toda *et al*., Engineering synthetic morphogen systems that can program multicellular patterning. *Science* **370**, 327–331 (2020). doi: 10.1126/science.abc0033; pmid: 33060357
45. K. A. Schwarz, N. M. Daringer, T. B. Dolberg, J. N. Leonard, Rewiring human cellular input-output using modular extracellular sensors. *Nat. Chem. Biol.* **13**, 202–209 (2017). doi: 10.1038/nchembio.2253; pmid: 27941759
46. I. Moraga *et al*., Synthekines are surrogate cytokine and growth factor agonists that compel signaling through non-natural receptor dimers. *eLife* **6**, e22882 (2017). doi: 10.7554/eLife.22882; pmid: 28498099
47. K. S. Stapornwongkul, M. de Gennes, L. Cocconi, G. Salbreux, J.-P. Vincent, Patterning and growth control in vivo by an engineered GFP gradient. *Science* **370**, 321–327 (2020). doi: 10.1126/science.abb8205; pmid: 33060356
48. Y. Ma, M. W. Budde, M. N. Mayalu, J. Zhu, R. M. Murray, M. B. Elowitz, Synthetic mammalian signaling circuits for robust cell population control. bioRxiv 278564 [preprint] (2020). doi: 10.1101/2020.09.02.278564
49. M. R. Bennett, D. Volfson, L. Tsimring, J. Hasty, Transient dynamics of genetic regulatory networks. *Biophys. J.* **92**, 3501–3512 (2007). doi: 10.1529/biophysj.106.095638; pmid: 17350994
50. S. H. Strogatz, *Nonlinear Dynamics and Chaos: With Applications to Physics, Biology, Chemistry, and Engineering* (Hachette, 2014).
51. K. J. Polach, J. Widom, A model for the cooperative binding of eukaryotic regulatory proteins to nucleosomal target sites. *J. Mol. Biol.* **258**, 800–812 (1996). doi: 10.1006/jmbi.1996.0288; pmid: 8637011
52. J. Miyazaki *et al*., Expression vector system based on the chicken β-actin promoter directs efficient production of interleukin-5. *Gene* **79**, 269–277 (1989). doi: 10.1016/0378-1119(89)90209-6; pmid: 2551778
53. H. Chassin *et al*., A modular degron library for synthetic circuits in mammalian cells. *Nat. Commun.* **10**, 2013 (2019). doi: 10.1038/s41467-019-09974-5; pmid: 31043592
54. D. T. Gillespie, A general method for numerically simulating the stochastic time evolution of coupled chemical reactions. *J. Comput. Phys.* **22**, 403–434 (1976). doi: 10.1016/0021-9991(76)90041-3
55. X. Pan, C. Dalm, R. H. Wijffels, D. E. Martens, Metabolic characterization of a CHO cell size increase phase in fed-batch cultures. *Appl. Microbiol. Biotechnol.* **101**, 8101–8113 (2017). doi: 10.1007/s00253-017-8531-y; pmid: 28951949
56. Q. Liu, D. J. Segal, J. B. Ghiara, C. F. Barbas 3rd, Design of polydactyl zinc-finger proteins for unique addressing within complex genomes. *Proc. Natl. Acad. Sci. U.S.A.* **94**, 5525–5530 (1997). doi: 10.1073/pnas.94.11.5525; pmid: 9159105
57. L. Bintu *et al*., Transcriptional regulation by the numbers: Applications. *Curr. Opin. Genet. Dev.* **15**, 125–135 (2005). doi: 10.1016/j.gde.2005.02.006; pmid: 15797195
58. E. Eden *et al*., Proteome half-life dynamics in living human cells. *Science* **331**, 764–768 (2011). doi: 10.1126/science.1199784; pmid: 21233346
59. B. Schwanhäusser *et al*., Global quantification of mammalian gene expression control. *Nature* **473**, 337–342 (2011). doi: 10.1038/nature10098; pmid: 21593866
60. K. L. Frieda *et al*., Synthetic recording and in situ readout of lineage information in single cells. *Nature* **541**, 107–111 (2017). doi: 10.1038/nature20777; pmid: 27869821
61. B. Schwalb *et al*., TT-seq maps the human transient transcriptome. *Science* **352**, 1225–1228 (2016). doi: 10.1126/science.aad9841; pmid: 27257258
62. J. J. Muldoon *et al*., Model-guided design of mammalian genetic programs. *Sci. Adv.* **7**, eabe9375 (2021). doi: 10.1126/sciadv.abe9375
63. J. A. Zitzewitz, O. Bilsel, J. Luo, B. E. Jones, C. R. Matthews, Probing the folding mechanism of a leucine zipper peptide by stopped-flow circular dichroism spectroscopy. *Biochemistry* **34**, 12812–12819 (1995). doi: 10.1021/bi00039a042; pmid: 7548036
64. M. Schlosshauer, D. Baker, Realistic protein-protein association rates from a simple diffusional model neglecting long-range interactions, free energy barriers, and landscape ruggedness. *Protein Sci.* **13**, 1660–1669 (2004). doi: 10.1110/ps.03517304; pmid: 15133165
65. S. Paulous, C. E. Malnou, Y. M. Michel, K. M. Kean, A. M. Borman, Comparison of the capacity of different viral internal ribosome entry segments to direct translation initiation in poly(A)-dependent reticulocyte lysates. *Nucleic Acids Res.* **31**, 722–733 (2003). doi: 10.1093/nar/gkf695; pmid: 12527782
66. E. Balleza, J. M. Kim, P. Cluzel, Systematic characterization of maturation time of fluorescent proteins in living cells. *Nat. Methods* **15**, 47–51 (2018). doi: 10.1038/nmeth.4509; pmid: 29320486
67. L. He, R. Binari, J. Huang, J. Falo-Sanjuan, N. Perrimon, In vivo study of gene expression with an enhanced dual-color fluorescent transcriptional timer. *eLife* **8**, e46181 (2019). doi: 10.7554/eLife.46181; pmid: 31140975
68. J. E. Ferrell Jr., S. H. Ha, Ultrasensitivity part II: Multisite phosphorylation, stoichiometric inhibitors, and positive feedback. *Trends Biochem. Sci.* **39**, 556–569 (2014). doi: 10.1016/j.tibs.2014.09.003; pmid: 25440716
69. J. E. Ferrell Jr., S. H. Ha, Ultrasensitivity part III: Cascades, bistable switches, and oscillators. *Trends Biochem. Sci.* **39**, 612–618 (2014). doi: 10.1016/j.tibs.2014.10.002; pmid: 25456048
70. J. A. Miller, J. Widom, Collaborative competition mechanism for gene activation in vivo. *Mol. Cell. Biol.* **23**, 1623–1632 (2003). doi: 10.1128/MCB.23.5.1623-1632.2003; pmid: 12588982
71. L. A. Mirny, Nucleosome-mediated cooperativity between transcription factors. *Proc. Natl. Acad. Sci. U.S.A.* **107**, 22534–22539 (2010). doi: 10.1073/pnas.0913805107; pmid: 21149679
72. N. E. Buchler, M. Louis, Molecular titration and ultrasensitivity in regulatory networks. *J. Mol. Biol.* **384**, 1106–1119 (2008). doi: 10.1016/j.jmb.2008.09.079; pmid: 18938177
73. C. Hsu, V. Jaquet, M. Gencoglu, A. Becskei, Protein Dimerization Generates Bistability in Positive Feedback Loops. *Cell Rep.* **16**, 1204–1210 (2016). doi: 10.1016/j.celrep.2016.06.072; pmid: 27425609
74. D. V. Israni, H.-S. Li, K. A. Gagnon, J. D. Sander, K. T. Roybal, J. Keith Joung, W. W. Wong, A. S. Khalil, Clinically-driven design of synthetic gene regulatory programs in human cells. bioRxiv 432371 [preprint] (2021). doi: 10.1101/2021.02.22.432371
75. T. Buder, A. Deutsch, M. Seifert, A. Voss-Böhme, CellTrans: An R Package to Quantify Stochastic Cell State Transitions. *Bioinform. Biol. Insights* **11**, 1–14 (2017). doi: 10.1177/1177932217712241; pmid: 28659714

ACKNOWLEDGMENTS

We thank M. Budde for suggestions on MultiFate circuit design; J. Tijerina at Caltech Flow Cytometry Facility for help with cell sorting; X. Wang and F. Horns for timely help with experiments during COVID and lab move; S. Xie for help with MultiFate-2 monoclone screening; S. Xie and S. Satia for advice on coding; J. Bois for teaching and sharing Caltech BE150 course materials for mathematical modeling; A. Khalil for suggestions on the choice of zinc fingers; R. Kuintzle, F. Horns, L. Chong, Z. Chen, M. Flynn, H. Klumpe, M. Budde, B. Gu, J. Gregrowicz, and E. Mun for critical feedback; and other members of the Elowitz lab for scientific input and support. **Funding:** Supported by DARPA (HR0011-17-2-0008, M.B.E.); the Allen Discovery Center program, a Paul G. Allen Frontiers Group advised program of the Paul G. Allen Family Foundation (UWSC10142, M.B.E.); the Spanish Ministry of Science and Innovation and FEDER (PGC2018-101251-B-I00, J.G.-O.); "Maria de Maeztu" Programme for Units of Excellence in R&D (CEX2018-000792-M, J.G.-O.); and the Generalitat de Catalunya (ICREA Academia program, J.G.-O.). M.B.E. is a Howard Hughes Medical Institute investigator. **Author contributions:** R.Z. and M.B.E. conceived of the project. R.Z. and M.B.E. designed experiments. R.Z. performed experiments. R.Z. and M.B.E. analyzed data. R.Z., J.M.d.R.-S., J.G.-O., and M.B.E. did mathematical modeling. R.Z. and M.B.E. wrote the manuscript with input from all authors. **Competing interests:** R.Z. and M.B.E. are inventors on a US provisional patent application related to this work. **Data and materials availability:** All DNA constructs (table S2) and cell lines (table S3) are available from M.B.E. or through the Addgene repository under a material agreement with California Institute of Technology. All data generated and all the computational and data analysis and modeling code used in the current study are available at data.caltech.edu/records/1882.

SUPPLEMENTARY MATERIALS

science.org/doi/10.1126/science.abg9765
Materials and Methods
Supplementary Text
Figs. S1 to S24
Tables S1 to S4
References (*55*–*75*)
MDAR Reproducibility Checklist
Movies S1 to S6

10 February 2021; accepted 29 November 2021
10.1126/science.abg9765

Synthetic multistability in mammalian cells

Ronghui ZhuJesus M. del Rio-SalgadoJordi Garcia-OjalvoMichael B. Elowitz

Science, 375 (6578), eabg9765. • DOI: 10.1126/science.abg9765

Building synthetic cell fate selection

An important goal for synthetic biology is to establish control systems that allow the direction of cells into multiple stable states, much like biological signaling systems do during organismal development. Zhu *et al*. devised a system that allows such control through designed zinc finger transcription factors that interact with one another through homo- and heterodimerization and can be regulated by small molecules that control dimerization and stability of the transcription factors (see the Perspective by Kunze and Khalil). Mathematical modeling allowed computational prediction of the system's behavior, and introduction of three designed transcription factors in cultured mammalian cells allowed direction of the cells into seven distinct, stable states. Understanding such multistability is useful in synthetic biology and can help to determine its roles in development and disease processes. —LBR